Schottky Barrier Photodiodes with Antireflection Coating

By M. V. SCHNEIDER

(Manuscript received July 19, 1966)

Schottky barrier diodes can be used for fast and efficient photodetectors if the incident light is coupled into the depletion layer of the diode and if electron-hole pairs are created by the internal photoelectric effect in the depletion layer. Fast response of the diode is achieved by designing a Schottky barrier with a small RC product. High quantum efficiency is obtained by coupling the light through a thin metal layer into the depletion region of the diode and by using an antireflection coating on the metal layer for matching the incident light beam.

Schottky barrier photodiodes have been made with thin semitransparent gold layers on n-type epitaxial silicon and with zinc sulfide as an antireflection coating. A net quantum efficiency of 70 percent has been achieved at the He-Ne laser wavelength of 6328 Å. The pulse response of packaged diodes with 0.5-nanosecond wide pulses shows a symmetrical pulse shape with only small distortion due to carrier diffusion and reactance in the completed package.

The diode structure is suitable for detector arrays. It is also useful for optical time domain reflectometry. The technique of coupling light through metal layers can be extended to other optical devices which require efficient transfer of radiation into a semiconductor through conducting electrodes.

I. DEFINITION OF THE SCHOTTKY BARRIER PHOTODIODE

A Schottky barrier is a rectifying metal-to-semiconductor contact with certain properties which have been originally described by Schottky.[1,2] The main feature of the Schottky barrier is that it has the properties of an ideal step junction and that only majority carriers are involved in the rectification process. Schottky barriers have been used for various devices in the microwave region. A few examples are the Au-n-type GaAs and the Au-n-type Si varactors described by Kahng and D'Asaro[3,4] and the honeycomb millimeter diode by Irvin and Young.[5] The Schottky

1611

barrier has not been used to any great extent for optical devices because of the difficult problem of coupling optical radiation through the metal contact into the semiconductor. The purpose of this paper is to present a solution to this problem and to describe the properties of a completed diode which will be defined as a Schottky barrier photodiode.

The Schottky barrier photodiode is a rectifying metal-to-semiconductor contact in which electron-hole pairs are created in the semiconductor by the internal photoelectric effect under incident illumination. The separation of the pairs is accomplished by the built-in electric field in the barrier or by an externally applied field across the barrier. The separation of the carriers leads to a photocurrent in the external circuit which may be amplified and detected. Internal amplification by avalanche multiplication cannot be achieved in a Schottky barrier photodiode because of nonuniform field intensities at the boundary of the metal-semiconductor interface.

II. STRUCTURE OF OPTICAL JUNCTION DETECTORS

Photodetectors with a high frequency response consist usually of a semiconductor p-n junction or a semiconductor p-i-n structure. A schematic drawing of such a detector is shown in Fig. 1. The incident radiation is absorbed in the intrinsic layer which is sandwiched between a p and an n-layer. Electron-hole pairs are created by the internal photoelectric effect and are separated by an applied electric field across the junction. Metal contacts are required on both sides of the structure in order to apply the electric field and to collect the carriers. The contacts on top of the p-layer shown in Fig. 1 are made in the form of stripes in order to transmit the incident radiation between adjacent stripes into the p-i-n region.
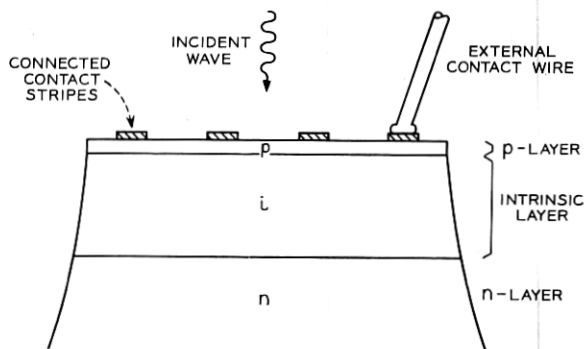

Fig. 1 — p-i-n photodiode with contact stripes on *p*-layer.

High quantum efficiency and fast response are achieved by proper choice of the semiconductor material and the physical dimensions of the layers including the contact stripes. Design criteria have been discussed by Anderson,[6] Lucovsky and Emmons,[7] and Riesz.[8] Internal multiplication with uniform and microplasma-free junctions with a guard ring has been achieved by Anderson, McMullin, D'Asaro and Goetzberger[9] and by Melchior and Lynch.[10]

A different approach is necessary for the case of a Schottky barrier photodiode shown in Fig. 2. A semitransparent metal is deposited on the surface of a semiconductor in order to create a surface barrier. The light is matched into the barrier by an antireflection coating which is
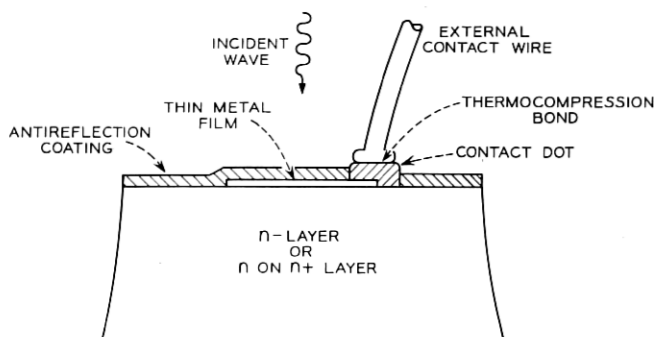

Fig. 2 — Schottky barrier photodiode with antireflection coating on metal film.

deposited on the semitransparent metal. A thick metal dot or a metal ring with a contact wire serves as an external contact for applying the dc back bias and for collecting carriers. The semiconductor material and the applied back bias are chosen in such a way that most of the carriers are created within the depletion layer. The net quantum efficiency of the device is determined mainly by the transmission loss in the metal film and by the quality of the antireflection coating. The response time is determined by the transit time of the carriers through the depletion layer and the RC product of the diode. Design criteria for achieving a small RC product will be discussed later in this paper.

Coupling of the incident light beam into the Schottky barrier can also be achieved by other means. Fig. 3 is a cross-sectional view of the Sharpless photodiode.[11,12] A point contact is formed on epitaxial material and the light is focused into the Schottky barrier through an etched dome in the semiconductor. An antireflection coating is not necessarily required because the semiconductor surface does not present a serious optical mismatch to the incident wave.
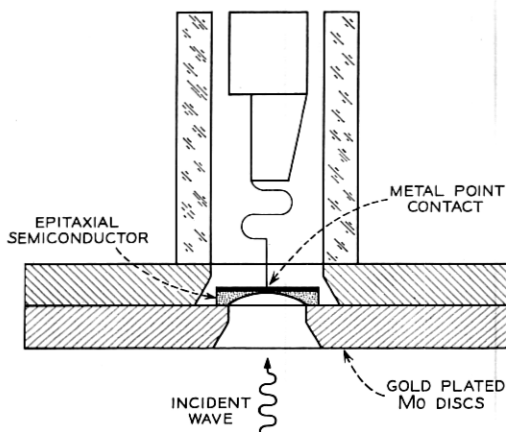
Fig. 3 — Point contact Schottky barrier photodiode with etched dome in epitaxial semiconductor.

Another way to build a Schottky barrier photodiode is shown in Fig. 4. A thick metal coating is applied to the semiconducting material. An array of slots or holes are etched into the metal. The holes are close to resonance at the wavelength of the incident radiation, e.g., they are approximately a quarter wavelength wide and are spaced approximately a half wavelength apart. The thickness of the metal has to be much smaller than a wavelength because the excited mode in the hole or the slot is under cutoff. The remaining reactive part of the surface impedance
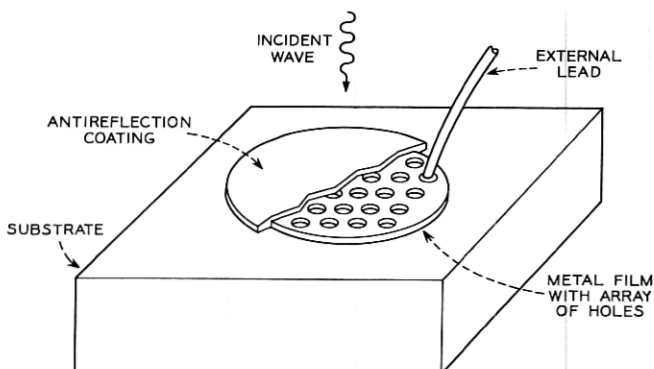

Fig. 4 — Photodiode or photodetector with metallic surface reactance sheet and antireflection coating.

of this structure is compensated by a suitable antireflection coating. This coating is only required for improving the final match of the device because a reactance sheet can be designed with a high return loss without any further matching elements.

Photodiodes of the type shown in Fig. 2 have been made on n-type epitaxial silicon for maximum response at the 6328 Å line of a He-Ne gas laser. Gold has been used for formation of the Schottky barrier and zinc sulfide for the antireflection coating. The results are discussed in the following sections of this paper. Various technological improvements in the technique of fabricating microarrays will have to be achieved in order to fabricate the photodiode shown in Fig. 4.

III. TRANSMISSION OF LIGHT THROUGH METAL FILMS

Metal films are characterized by high reflectivity and low transmission in the visible range of the spectrum. The transmission through the film can be increased by reducing its thickness. The reflection can be decreased by a dielectric film acting as a quarter wave transformer on top of the metal film. These two simple steps make it possible to transmit light into an optical device which requires metal electrodes.

Optical constants of thin metal films are listed by Schopper,[13] Heavens,[14] and Mayer.[15] The physical theory and measurements are described by Parker Givens[16] and by Abelès.[17] A marked dependence of the optical constants on film thickness is observed. Other parameters of importance include the technique used in the deposition process, the substrate temperature, deposition rate and surface properties of the substrate. A typical example of steps taken in substrate preparation, purity of materials and pressures observed in the vacuum chamber is described by Bennett and Ashley[18] and a review on nucleation and film growth as a function of various parameters is given in a paper by Behrndt.[19] What complicates matters for device applications is the fact that the films may not be continuous and that the index of refraction depends on the angle of incidence as described by Hall.[20]

These difficulties do not prevent the fabrication of an antireflecting metal-semiconductor surface. Fairly consistent results can be achieved with gold evaporated from tungsten or molybdenum boats under high vacuum or ultra-high vacuum conditions. The optical surface impedance of the structure can be measured and from this one can determine a unique dielectric constant and a unique thickness which will allow optical matching at a specified wavelength. The steps in this procedure are similar to matching microwave networks by using the Smith Chart.

The reflectance and the transmittance which one can expect from a thin gold film at $\lambda = 6328$ Å are shown in Fig. 5. Reflectance, transmittance and loss are plotted as a function of film thickness for an unsupported Au film with an index of refraction $N = n - j \cdot k = 0.30 - j \cdot 3.0$. The only assumptions used in this plot are that one deals with normal incidence and that this particular index of refraction is independent of the film thickness. The index $N = 0.30 - j \cdot 3.0$ is an approximate value for bulk gold obtained from measurements described by Parker Givens.[16] Other data for gold deposited under various conditions and listed by Schopper[13] cover an approximate range of $n = 0.30 \pm 0.10$ and $k = 3.0 \pm 1.0$ at wavelengths in the range from 6000 Å to 6600 Å.

The exact thickness of a thin metal film is usually of secondary importance for many device applications. What one needs to know for devices described in this paper is reflectance, transmittance, and loss for a specified surface resistance (sheet resistance) of the film. The surface resistance of the film limits the frequency response of the device because it will contribute to the resistive part of the device. The relationship between the surface resistance and the RC product will be discussed later.

Fig. 6 is a plot of reflectance, transmittance and loss measured for Au films at $\lambda = 6328$ A for surface resistances in the 3 to 6 ohm/square range. The Au films are deposited on fused quartz slides under the following conditions:

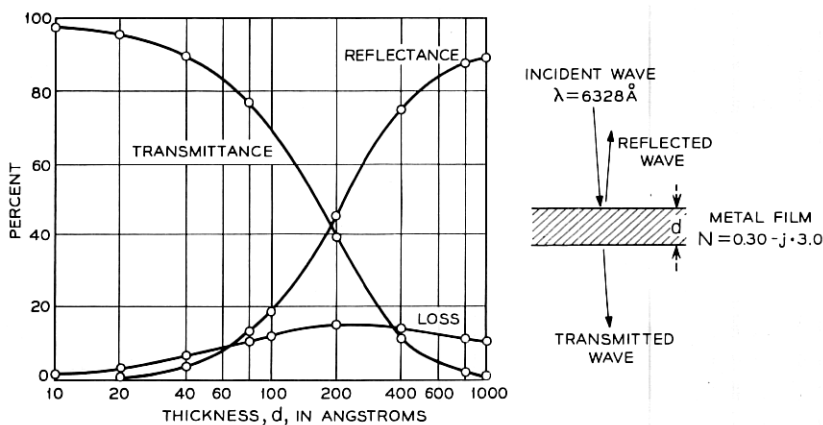(i) The substrates are cleaned ultrasonically in successive baths

Fig. 5 — Transmittance, reflectance, and loss for thin metal film with $N = 0.30 - j \cdot 3.0$.
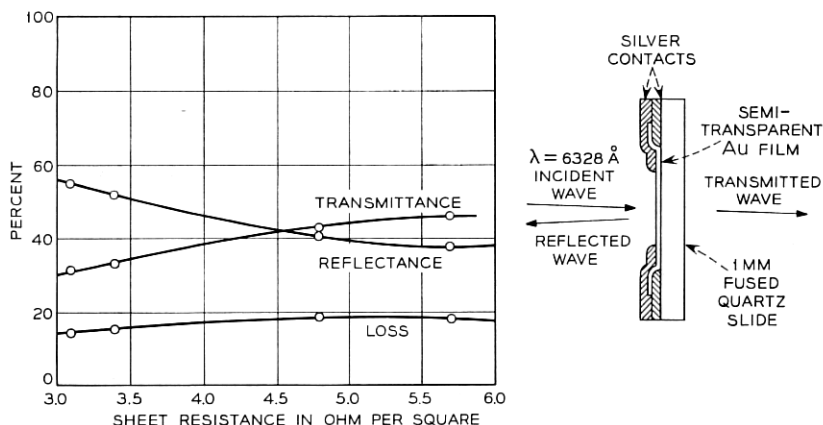
Fig. 6 — Transmittance, reflectance, and loss of evaporated gold films on fused quartz substrates.

of a detergent, distilled water and alcohol. They are dried with tank nitrogen and vapor degreased in isopropyl alcohol in the apparatus described by Holland.[21]

(ii) The substrate is transferred into a VE-400 (Vacuum Electronics, Inc.) vacuum system which is pumped down to a pressure of $2 \cdot 10^{-7}$ torr. Due to the location of the ionization gauge, which is between the diffusion pump and the liquid nitrogen cold trap, the pressure in the bell jar is an order of magnitude higher.

(iii) Gold is evaporated from a tungsten coil located 6 inches from the substrate with estimated deposition rates in the range of 5 to 10 Å/sec. The quartz substrate is not heated.

(iv) The dc resistance of the film is continuously monitored during evaporation with two silver contacts shown in Fig. 6. Additional silver contacts are applied immediately after the gold evaporation in order to sandwich the gold layer between two layers of silver. This method insures minimum contact resistance between the silver and the gold. All three layers (Ag, Au, Ag) are applied consecutively without opening the vacuum system.

The thickness of the films is measured with a multiple beam interferometer; e.g., the film with a 5.7 ohm/square sheet resistance has a thickness of 180 ± 15 Å. This particular sheet resistance is approximately 4.5 times higher than that which one would obtain from the resistivity ρ of bulk gold for a thickness of 180 Å ($\rho = 2.44 \times 10^{-6}$ ohm cm at room temperature). One of the reasons for this discrepancy is the

fact that conduction in thin films depends upon the scattering from the film boundaries. This means that bulk resistivities cannot be achieved for thin films. Another effect of importance is that the film may be discontinuous; that means the film consists of a number of islands with partial bridging between adjacent islands as described by Chopra[22] and Francombe and Sato.[23] The optical properties of such a film can be characterized by a complex index of refraction provided that the average distance between neighbouring islands is a small fraction of the optical wavelength.

The reflectance and transmittance curves shown in Fig. 5 are calculated for a metal film which is not supported by any substrate. Fig. 7 is a similar plot for a film supported by a substrate with an index of refraction $N = 3.75$. This particular index corresponds approximately to silicon with $N = 3.75 - j \cdot 0.18$ at $\lambda = 6328$ Å. Comparison with Fig. 5 shows that the reflectance for a specified film thickness is higher. The loss in the metal film is lower because of the increased reflectance. Reflectance, transmittance, and loss are the same for very thick films as shown by the calculated points for $d = 1000$ Å.

IV. OPTICAL MATCHING OF A METAL-SEMICONDUCTOR CONTACT

A metal-semiconductor contact can be optically matched at a specified wavelength if the reflection coefficient or the surface impedance is known for that particular wavelength.
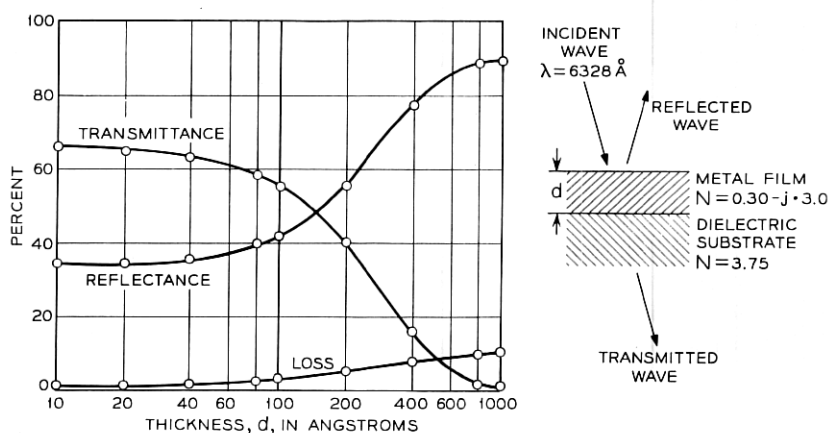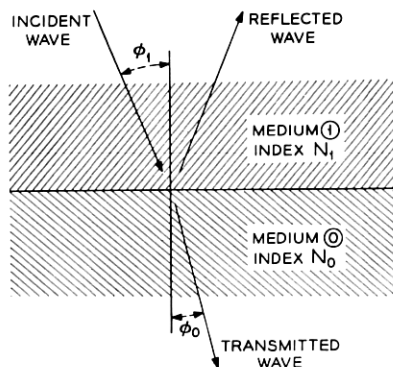

Fig. 7 — Transmittance, reflectance, and loss of metal film on dielectric substrate.

The reflection coefficient r_1 at the interface of two media in Fig. 8 is given by

$$r_1 = \frac{g_1 - g_0}{g_1 + g_0}. \tag{1}$$

The quantities g_k $(k = 0, 1)$ are generalized impedances or admittances (immittances) of the two media and μ_k $(k = 0, 1)$ is the permeability

Fig. 8 — Plane wave reflected and transmitted from plain boundary.

of the medium. The immittance is directly related to the index of refraction of that particular medium. The transmission coefficient t_1, is

$$t_1 = \frac{2g_1}{g_1 + g_0}. \tag{2}$$

Equations (1) and (2) are exactly identical with the equations used for computing the voltage or current reflection coefficient and the transmission coefficient for two adjacent RF transmission lines at different impedance levels.

A sequence of plane parallel films can be treated by applying (1) and (2) with a recursion formula which takes into account the phase shift between two adjacent media. The exact procedure is derived by Wolter.[24] The result with a sequence of three media for the reflection coefficient r_2 and the transmission coefficient t_2 is

$$r_2 = \frac{(g_2 - g_1)(g_1 + g_0)\exp(\rho_1 d_1) + (g_2 + g_1)(g_1 - g_0)\exp(-\rho_1 d_1)}{(g_2 + g_1)(g_1 + g_0)\exp(\rho_1 d_1) + (g_2 - g_1)(g_1 - g_0)\exp(-\rho_1 d_1)} \tag{3}$$

$$t_2 = \frac{4g_1g_2}{(g_2 + g_1)(g_1 + g_0) \exp{(\rho_1 d_1)} + (g_2 - g_1)(g_1 - g_0) \exp{(-\rho_1 d_1)}} \tag{4}$$

with the notation shown in Fig. 9. The quantities g_k are again the immitances of the media. The exponential term $\exp{(\pm\rho_1 d_1)}$ represents the phase shift between the two adjacent boundaries shown in Fig. 9.

Equations (3) and (4) are valid if the impedance or admittance of the center medium is complex; e.g., if it is a metal. A plane wave launched in medium 2 will excite a hybrid wave in medium 1; that means planes of equal phase and of equal amplitude will not coincide unless one deals with normal incidence. A wave with parallel planes for equal phase and equal amplitude can be propagated in an absorbing medium. Such a wave, however, cannot be excited by a plane wave coupled into the absorbing medium through a plane boundary at an oblique angle. This property leads to an index of refraction which is a function of the angle of incidence. Further details may be found in the original work by Fry.[25,26]

The reflection coefficient r_2 in (3) should be made as small as possible for building devices with a high transmission into the substrate. This cannot be achieved for a metal-semiconductor structure. It is possible, however, to deposit an additional film on the metal and to compensate the complex reflection coefficient by proper choice of the index of refraction and the thickness of this antireflection coating. The surface impedance on top of medium 1 in Fig. 9 which represents the metal is

$$G_0 = U - j \cdot V = \frac{1 - r_2}{1 + r_2} \tag{5}$$

with U being the real part and jV the complex part of the surface impedance. G_0 can be matched to an impedance G_2 by a dielectric layer with a proper thickness D and a proper impedance G_1 if

$$G_1^2 = G_2 \left\{ \frac{V^2}{U - G_2} + U \right\} \tag{6}$$

$$D = \frac{\lambda}{2\pi n} \arctan \left(\frac{G_1}{G_2} \cdot \frac{U - G_2}{V} \right). \tag{7}$$

The notation is shown in Fig. 10. The quantity n is the index of refraction of the dielectric material. For an interface with a real surface impedance $G_0 = U$, one obtains with $V = 0$ from (6) and (7)

$$G_1 = \sqrt{G_0 G_2} \tag{8}$$
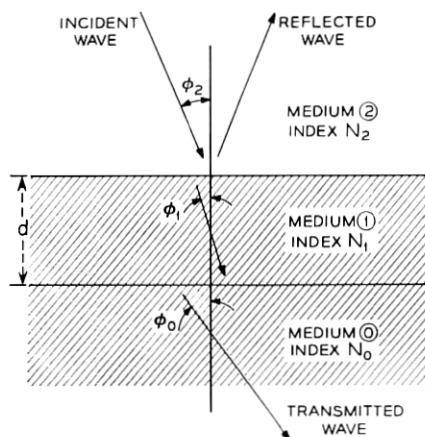
Fig. 9 — Reflection and transmission for 3 media.

$$D = \frac{1}{n} \cdot \frac{\lambda}{4} . \tag{9}$$

This is the well-known relationship for a quarter-wave transformer connecting microwave transmission lines at different impedance levels. The wavelength λ is the vacuum wavelength.

A practical example is treated in Fig. 11. Reflection coefficients for a Au-Si structure are plotted in the complex plane for a gold layer with a thickness of 100 Å and 200 Å. The example refers to normal incidence at a wavelength of $\lambda = 6328$ Å. It is assumed that the index of refraction is $N_1 = 0.28 - j \cdot 3.01$ for gold and $N_0 = 3.72 - j \cdot 0.18$ for silicon. The index of refraction and the thickness of the antireflection coating are listed in Table I.
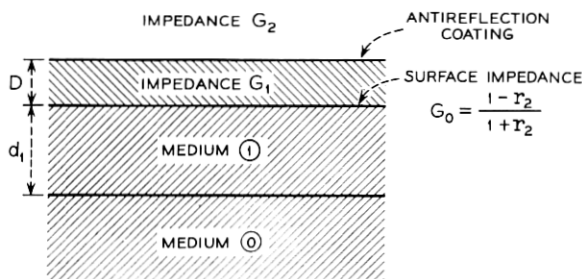

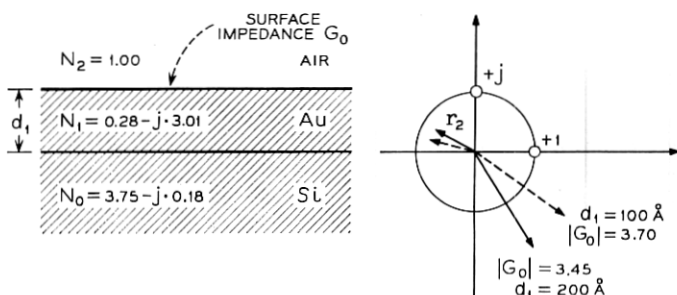Fig. 10 — Impedance matching with antireflection coating on medium No. 1.

Fig. 11 — Surface impedance of gold-silicon Schottky barrier at $\lambda = 6328$ A.

The loss in the gold film and the reflectance and the transmittance of the complete structure is shown in Fig. 12 and Fig. 13. All three quantities are plotted as a function of the thickness of the gold film for two *fixed* antireflection coatings with $n = 2.30$, $D = 500$ Å and $n = 3.30$, $D = 240$ Å. Minimum reflectance is achieved as predicted in Table I. All curves are obtained by applying (3) and (4) with a recursion formula for one additional layer.

The conclusion from the results of Figs. 12 and 13 is that transmission with low loss into the silicon substrate is feasible.

The reflectance achieved for three evaporation processes with zinc sulfide deposited on a Au-Si surface barrier is shown in Fig. 14. Gold layers with sheet resistances in the range of 6 ohm/square are first evaporated on epitaxial silicon. Zinc sulfide is evaporated on the gold layer. The return loss at $\lambda = 6328$ Å is continuously measured with an optical reflectometer and a He-Ne laser as a signal source. The reflectometer is similar to the one described by Perry.[27] The measured return loss is calibrated in dB. The evaporation is continued after reaching the first minimum in one case in order to show the periodicity of the process. One concludes that an improvement of 8 dB to 9 dB in return loss is possible with a single layer of zinc sulfide. The return loss without the matching layer is 3 dB. The total return loss is therefore, 11 dB to 12 dB.

TABLE I

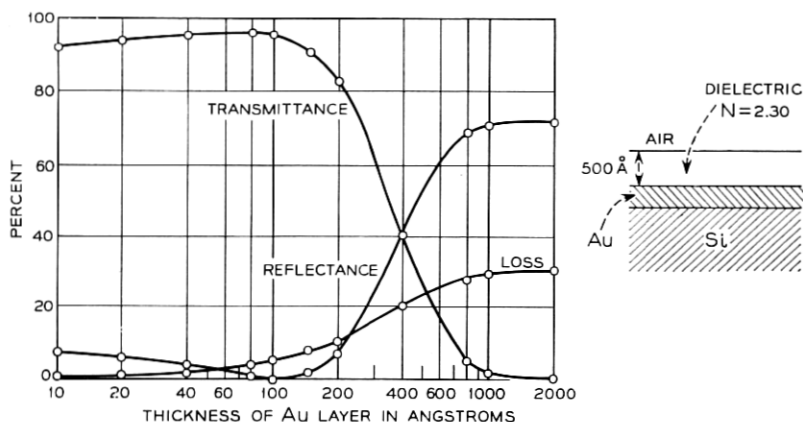| Thickness of Au Film	Index n of Coating	Thickness of Coating in Å	Thickness of Coating in Terms of Phase Angle
100 A	2.28	510 A	66°
200 Å	3.33	242 Å	46°

Fig. 12 — Reflectance, transmittance, and loss from Au-Si surface barrier with 500 Å thick ZnS antireflection coating.

It is difficult to measure the transmittance or the loss in the metal for a ZnS-Au-Si structure. Some indication may be obtained from the measurement of the net quantum efficiency of the device if all the carriers can be collected and if there is no internal multiplication. Another direct method is to use the fact that the losses in the metal will increase its temperature and change its resistance. The resistance changes could be simulated by obtaining the same increase with a dc current flowing in
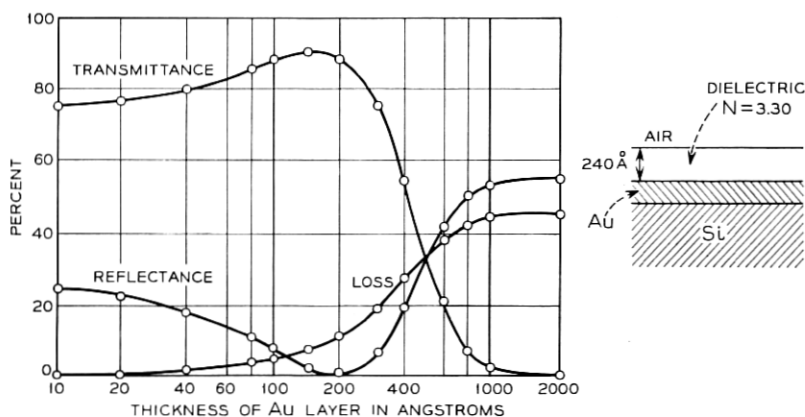

Fig. 13 — Reflectance, transmittance, and loss from Au-Si surface barrier with 240 Å thick ZnS antireflection coating.
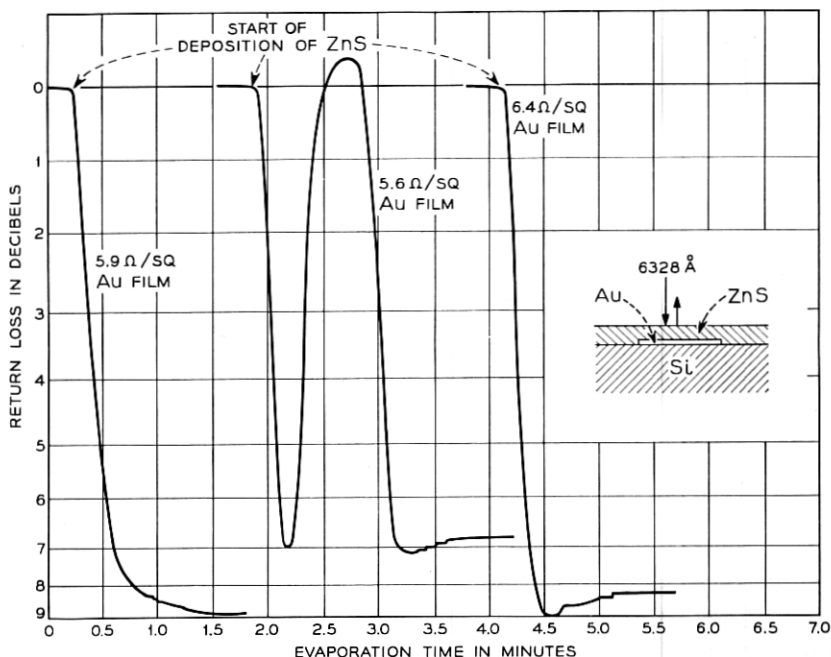
Fig. 14 — Return loss from Si-Au surface barrier during deposition of antire-flection ZnS layer.

the Au film. The same procedure is used for power detector calibrations in the microwave frequency range.

The transmittance through Au-ZnS has been measured for a slightly modified case shown in Fig. 15 using a 1-mm thick quartz slide as a substrate. A 5-ohm/square Au film is evaporated on the quartz. The reflectance is 40 percent and the transmittance is 43 percent at 6328 Å as shown in Fig. 6. Zinc sulfide is then evaporated on the Au. The return loss and the transmission are continuously measured with a double reflectometer at $\lambda = 6328$ Å mounted inside the vacuum system. The double reflectometer records transmitted and reflected power simul-taneously as shown by the coincidence of maxima and minima on the time scale in Fig. 15. The calibration in dB is obtained with a set of standard optical attenuators. The results from this experiment are

(i) The transmittance is improved by 2.5 dB. This means that 76 percent of the incident light is transmitted.

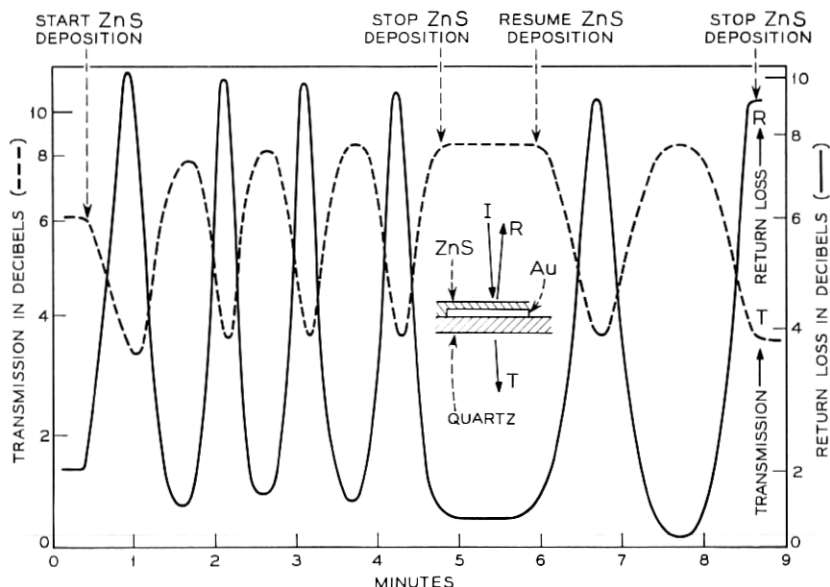(ii) The reflectance is decreased by 10 dB which means that the reflectance is reduced from 40 to 4 percent.

Fig. 15 — Return loss and transmission of gold film on quartz substrate during deposition of ZnS antireflection coating.

(iii) The process is periodic which means the losses in the ZnS are small.

(iv) The evaporation process can be interrupted at any time and resumed later without changing the periodicity of the process and the levels of the minima and the maxima.

V. DESIGN OF THE SCHOTTKY BARRIER PHOTODIODE

5.1 *Optical Absorption and Carrier Generation in the Schottky Barrier*

The absorption coefficient α of the semiconductor and the width of the depletion layer w are important parameters for designing a Schottky barrier photodiode. The reason for this is as follows. The photocurrent through the depletion layer consists of two contributions. One is due to the carriers created within the layer, the other is due to carriers generated in the adjacent bulk material which diffuse later into the junction. Minority carriers which enter the junction by diffusion will be swept across the junction by the applied external field. This diffusion current may lead to delay distortion if the incident wave is pulsed or rf modu-

lated. The diffusion current is small if most of the optical power is absorbed within the depletion layer. This requires

$$w \gg \frac{1}{\alpha}. \tag{10}$$

The upper limit for w is determined by the transit time which can be tolerated for the carriers.

The absorption coefficient α of Ge and Si as a function of wavelength is given in Fig. 16. The width of the depletion layer in a uniformly doped material with a carrier concentration N under an applied external voltage V is given by Kahng[3,28] as
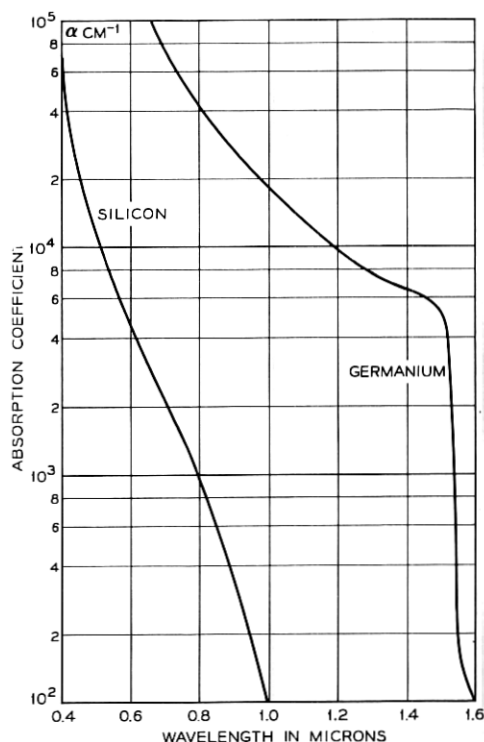
$$w = \sqrt{\frac{2\varepsilon(V_D + V)}{qN}} \tag{11}$$

Fig. 16 — Optical absorbtion coefficient of silicon and germanium at 300° K.

where V_D is the diffusion potential, ε the dielectric constant and q the electron charge. The diffusion potential is the potential difference of the conduction band level between its value at the surface and its value inside the bulk material. Diffusion potentials of various metal-semiconductor combinations can be obtained from data supplied by Cowley and Sze.[29] The diffusion potential in a Schottky barrier photodiode is usually much smaller than the applied back bias V because of the requirement $w \gg 1/\alpha$. With $q = 1.60 \times 10^{-19}$ coulomb and $\varepsilon = 8.85 \times 10^{-14} \, \varepsilon_r$ farad/cm one obtains

$$w = 1.05 \times 10^7 \sqrt{\frac{\varepsilon_r (V_D + V)}{N}} \text{ micron.} \quad (12)$$

N is the doping level in carriers/cc and w is measured in μm or micron ($1 \, \mu$m $= 10^{-4}$ cm). The ratio of capacitance C to junction area A is

$$\frac{C}{A} = \frac{\varepsilon}{w} = \sqrt{\frac{\varepsilon q N}{2(V_D + V)}}. \quad (13)$$

The width of the depletion layer for Ge and Si as a function of the total voltage $V_D + V$ is shown in Figs. 17 and 18. The breakdown limit
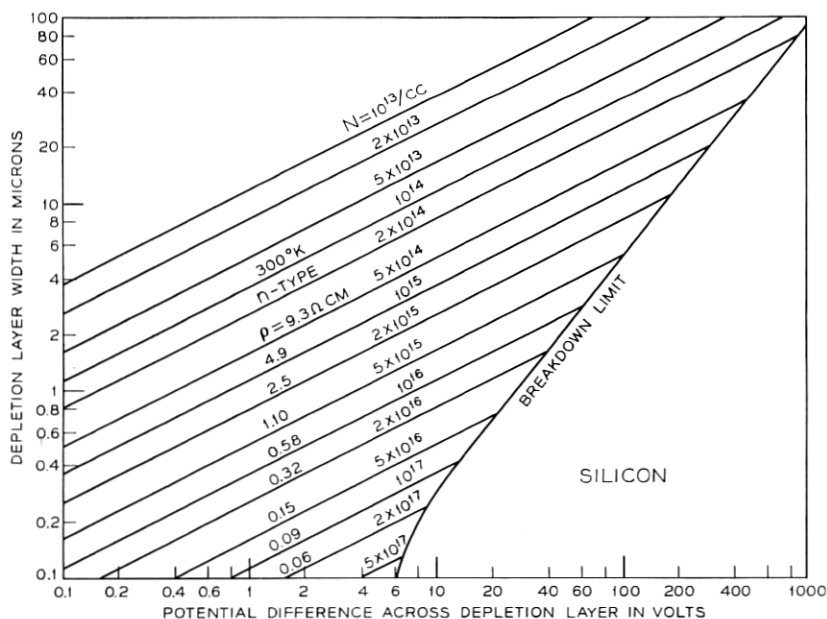

Fig. 17 — Depletion layer width in n-type silicon as a function of potential difference $V + V_D$ across depletion layer.
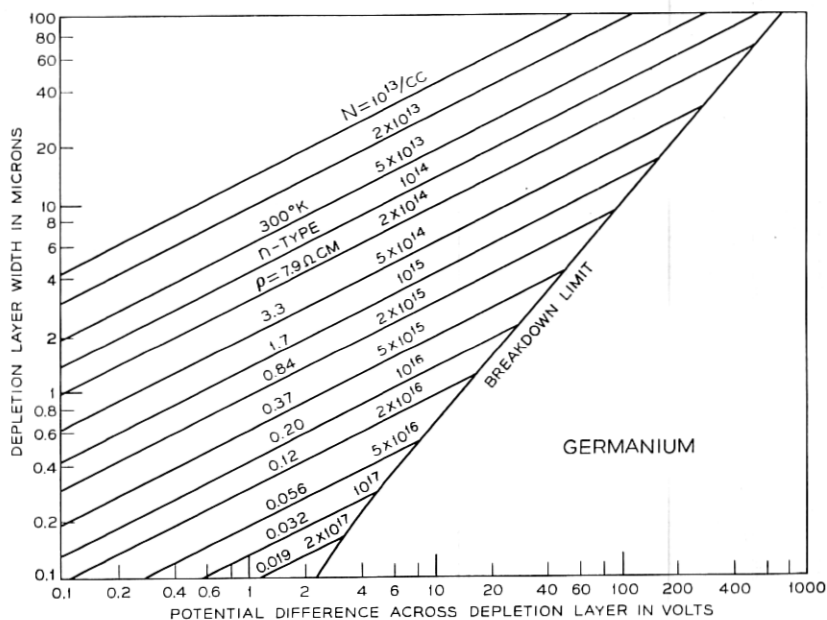
Fig. 18 — Depletion layer width in n-type germanium as a function of potential difference $V + V_D$ across depletion layer.

refers to an abrupt junction in the bulk. It is desirable that the depletion width satisfy (10). Moreover, for any particular application, the thickness w should be no thinner than is necessary to achieve a cutoff frequency which is twice the maximum operating frequency since the maximum available power from a photodiode depends inversely upon the square of the diode capacitance. It is not always possible to satisfy these requirements because of transit time considerations or because of material properties. The drift current for a specified depletion layer width w is

$$J_{\text{Drift}} = q\varphi(1 - e^{-\alpha w}) \tag{13}$$

where φ is the incident photon flux at the front of the depletion layer and q the electron change. One obtains e.g., for $w = 2/\alpha$ a value of 0.86 for the reduction factor $1 - \exp(-\alpha w)$. The total current will be larger because 14 percent of the radiation will be absorbed beyond the depletion layer in the bulk material and create diffusion current. The exact amount of diffusion current under static condition may be found in a paper by Gärtner.[30]

5.2 Frequency Limitations of the Photodiode

The frequency limitations for Schottky barrier photodiodes are determined by the transit time of the carriers through the depletion layer, the sheet resistance of the metal film, the resistance of the bulk material and the capacitance of the junction.

The transit time for a carrier depends on the type of carrier and the location of its origin within the depletion layer. The carriers may reach saturation velocities for sufficient high field intensities; e.g., 10^7 cm/sec for electrons in silicon. The holes will move at lower velocities. One has to remember, however, that holes are created predominantly in the high field region in the vicinity of the metal and will travel only a short distance to the metal electrode. Electrons will have to travel over a much longer distance and through a region of low field intensities as shown in Fig. 19. The electron transit time τ_{el} will thus be the predominant factor. This transit time has been calculated by B. C. DeLoach[31] by assuming that

(i) electrons reach the saturation velocity v_s at the maximum field in the junction, and

(ii) the transit of the carrier through the junction is completed when it reaches the field $E_o = kT$, that means when it joins the free carriers with an average energy kT (0.026 eV at 300°K) to the right of the swept space charge.
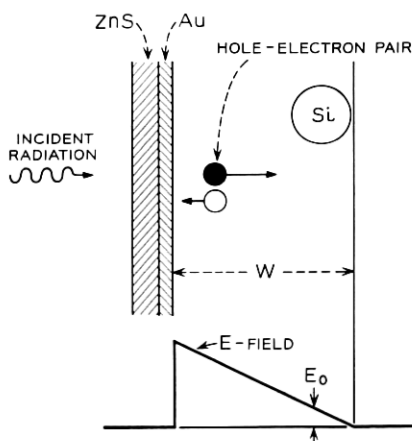

Fig. 19 — Pair creation under incident illumination with electric field intensity E in depletion layer.

The result for the electron transit time τ_{el} is

$$\tau_{el} = \frac{w}{v_s}. \tag{14}$$

Typical values which may be achieved in a silicon surface barrier are $w = 5$ microns and $v_s = 10^7$ cm/sec. This leads to an electron transit time $\tau_{el} = 5.10^{-11}$ sec. The corresponding cutoff frequency is $f_c = 1/\tau_{el} = 20$ GHz.

The frequency response of a photodiode with a capacitance C per unit area and a sheet resistance R_s has been calculated by Lucovsky and Emmons.[32] The cutoff frequency depends on the geometry of the diode and in particular on the location of the ohmic contact. Three types of contacts shown in Fig. 20 have been discussed by the authors. The 3-dB cutoff frequencies for the short circuited diodes are

$$\omega_c = \frac{3}{R_s C b^2} \qquad \text{linear contact} \tag{15}$$

$$\omega_c = \frac{8}{R_s C a^2} \qquad \text{ring contact} \tag{16}$$

$$\omega_c = \frac{4}{R_s C \cdot F(a,b)} \qquad \text{dot contact} \tag{17}$$

with

$$F(a,b) = \frac{a^2}{2} - \frac{3b^2}{2} + \frac{2b^4}{b^2 - a^2} \log \frac{b}{a}. \tag{18}$$

The dimensions a,b are defined in Fig. 20. The formulas have been derived for a p-n photodiode with the p-layer as the conducting layer. They remain fully valid if the p-layer is replaced by a thin metal film with a sheet resistance of R_s ohm/square. The cutoff frequency for the

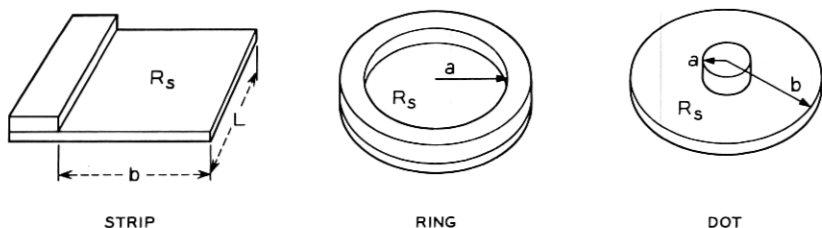
STRIP   RING   DOT

Fig. 20 — Contact shapes for ohmic contacts on thin metal film of Schottky barrier photodiode.

linear contact shown in Fig. 20 is independent of the dimension L because identical diodes connected in parallel will display the same frequency response if they are operated under short circuit conditions.

All three types of contacts can be used for Schottky barrier photodiodes. Ring contacts will give the highest cutoff frequencies for a specified diode area and given material properties. The fabrication of dot contacts is simpler because the ring contact has to be deposited by masking off the center area of the diode for the deposition of the contact ring. Dot contacts can be evaporated through an ordinary metal mask with an array of holes. This makes dot contacts particularly useful for photodiode arrays or for the fabrication of a large number of photodiodes on a single wafer which can be sliced up later. It is convenient to set the contact dot off center in order to facilitate the attachment of an external connection without interfering with the incident light beam. This is shown in Fig. 21. The large dots are semitransparent gold films on Si with a diameter of 10 mils and a sheet resistance of 5 to 7 ohm/square. The small contact dots have a diameter of 3 mils. The capacitance of each diode for a substrate material with a resistivity of 2.7 ohm cm at a back bias of 60 volt is 0.9 to 1.0 pF. The cutoff frequency cannot be calculated from (17) for the dot contact because the contact in Fig. 21 is off centered. A good approximation is obtained by applying (15) for the linear contact with b being the diameter of the semitransparent gold film. The cutoff frequency obtained for this particular diode at the specified back bias of 60 volt is $f_c = \omega_c/2\pi = 22$ GHz. This cutoff is of the same order as the cutoff frequency obtained from transit time considerations.
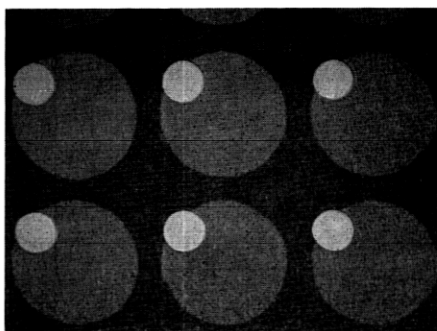

Fig. 21 — Array of Schottky barrier photodiodes on epitaxial silicon wafer before deposition of antireflecting coating. The diameter of the large semitransparent gold dots is 0.25 mm, the diameter of the small gold contact dots is 0.075 mm.

VI. FABRICATION AND PACKAGING OF Si-Au-ZnS PHOTODIODES

The combination of materials for Schottky barrier photodiodes depends on the frequency range of the incident radiation and the metallurgical properties of the metal-semiconductor system. Silicon and germanium are both suitable for the visible range of the spectrum. Stable Schottky barriers can be formed with a number of other metals, e.g., Ag, Al, Pt, and Ni. The eutectic temperatures of the various metal-semiconductor combinations determine the maximum device temperature. The eutectic temperature of Au-Si is 370°C. The choice of the matching coating is governed by the optical surface impedance of the metal-semiconductor combination. A total optical return loss of 12 dB can be achieved with ZnS which has a dielectric constant $\varepsilon_r = 2.3$. A higher return loss may be desirable; however, the stability of ZnS and the good adherence to the Au is an advantage compared to other dielectric materials.

The surface preparation of the semiconductor substrate is relatively simple. Epitaxial silicon wafers n on n^+ with alloyed gold antimony back contacts are rubbed with a clean cotton swab under methanol, boiled in distilled water, etched in HF, washed in distilled deionized water, washed in methanol and finally dried with nitrogen. The wafer is covered with a molybdenum mask with an array of 10-mil diameter holes. Only $\frac{2}{3}$ of the wafer are covered by this mask. The remaining $\frac{1}{3}$ of the wafer is later used for test purposes of the optical return loss during the evaporation of the antireflection coating. The unit is transferred into the vacuum system which is pumped down to a pressure of 2–3 $\times$ 10^{-7} torr measured at its pumping port. Gold is evaporated from a tungsten coil. The sheet resistance of the gold is measured on a 1-mm quartz slide which is located adjacent to the silicon wafer. The evaporation is discontinued when the sheet resistance measured on the quartz slide is in the range of 5 to 7 ohm/square. Separate measurements have shown that the sheet resistance of the Au on the Si wafer is also in the 5 to 7 ohm/square range.

A second deposition of Au through a molybdenum mask with an array of 3-mil holes is made on the wafer. The 3-mil Au dots are needed later for contacting purposes. A photograph of the semitransparent Au dots and the contacting 3-mil dots is shown in Fig. 21. The second mask is removed after the Au evaporation and the unit is mounted in a vacuum system which is equipped with an optical reflectometer at $\lambda = 6328$ Å. Zinc sulfide is evaporated on the wafer. The reflectance from the test area on the wafer is measured continuously and the evaporation is

stopped at the first maximum of the return loss. Typical results obtained from the reflectometer recording are shown in Fig. 14.

The step of depositing 3-mil Au contacts is repeated in order to facilitate thermocompression bonding to the contact area. The second mask is mounted in exact registry with the first evaporation of contact dots. This means that a ZnS layer is sandwiched between two identical contact dots. This layer is shorted out after completion of the thermocompression bonding process of a 1-mil Au wire to the contact dot. Fig. 22 is a photograph of the wafer surface after completion of all evaporation processes. The wafer surfaces shown in Figs. 21 and 22 are both illuminated from a standard tungsten lamp for obtaining the photographs.

A cross sectional view of the detector packaged into a modified type N connector body is shown in Fig. 23 and a photograph of the completed structure in Fig. 24. A metallized quartz washer is used for electrical separation of the diode terminals. A bypass capacitor provides an RF short between the outer conductor of the connector body and the terminal which is connected to the metal side of the Schottky barrier. Various parts of the package are identified in the figure caption.

VII. MEASUREMENT OF PULSE RESPONSE AND NET QUANTUM EFFICIENCY

The pulse response of packaged Schottky barrier photodiodes has been examined by phase locking the TEM_{00q} modes of a 6328 Å He-Ne gas laser with an internal phase modulator. The laser output consists of pulses with a half width of approximately 0.5 nanoseconds separated by 11 nanoseconds. The average optical power is 0.3–0.4 milliwatt.

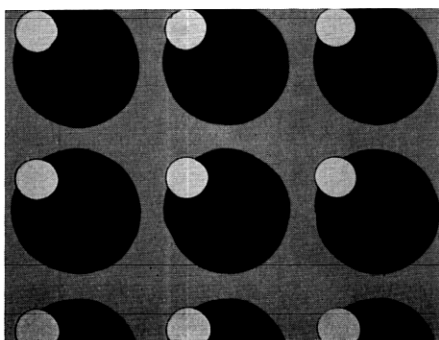A typical pulse response obtained with a completed photodiode dis-

Fig. 22 — Array of Schottky barrier photodiodes on epitaxial silicon wafer after deposition of the antireflecting coating. The dot dimensions are the same as in Fig. 21.
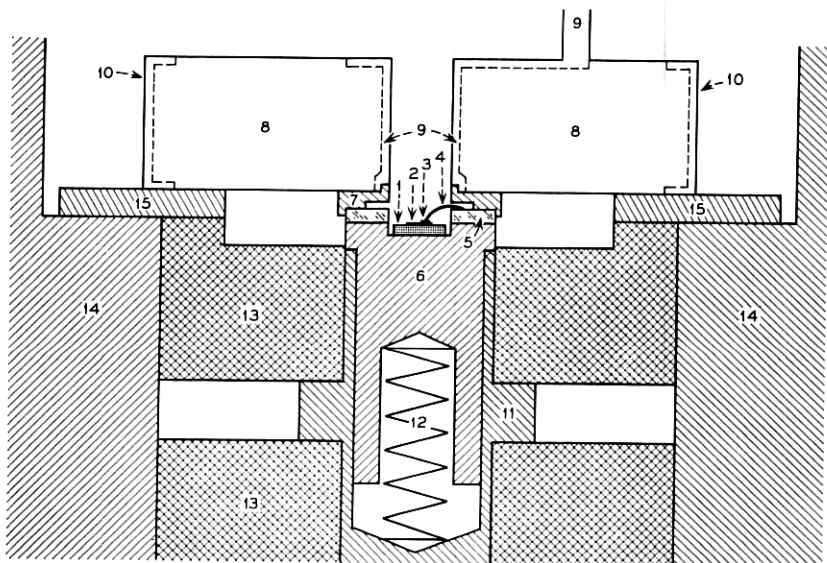
Fig. 23 — Cross-sectional view of diode package. (1. Silicon wafer. 2. Thin gold film. 3. Thermocompression bond on gold contact. 4. Contact wire to quartz washer. 5. Quartz washer, top and bottom are metallized. 6. Brass pin. 7. Brass adapter ring. 8. Bypass button capacitor 1000 pF. 9. Inside metal connection of button capacitor and external lead for applying dc bias to photodiode. 10. External metal connection of button capacitor. 11. Brass pin forming part of center conductor of the connector. 12. Steel spring. 13. Teflon spacers. 14. Connector body. 15. Steel washer.)
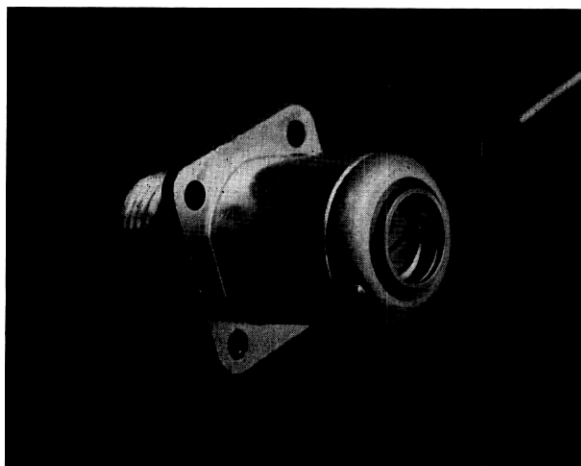

Fig. 24 — Completed diode package showing connector body and external lead wire for dc bias.

played on a Tektronix sampling oscilloscope Type 661 with a rise time of 0.1 nsec is shown in Fig. 25. The diode is made on 2.7-ohm cm epitaxial silicon with the 10-mil diameter dots shown in Figs. 21 and 22. The half width of the pulses is 0.45 nsec at a back bias of 50 volts. The net quantum efficiency measured with an Eppley thermocouple #4952 as a reference is 70 percent. This efficiency is obtained by graphical integration of the pulse shape shown in Fig. 25 and by assuming that the diode acts like an ideal current source into the 50-ohm broadband load of the sampling oscilloscope.

A close inspection of the pulse shape shows that the leading edge is slightly steeper than the trailing edge. The distortion in the trailing edge is due to diffusion current and to case capacitance in the package. The influence of the diffusion current can be examined by observing the pulse shape for various back bias conditions. Fig. 26 is the pulse response of the same diode at a back bias of 0, 4, 15, and 50 volt. A diffusion tail is clearly visible at a back bias of 0 volt and 4 volt. The diffusion tail is depressed at higher back bias because more carriers are created within the depletion layer.

An important property required for many practical applications is a uniform response of the photodiode over the entire area of the junction.
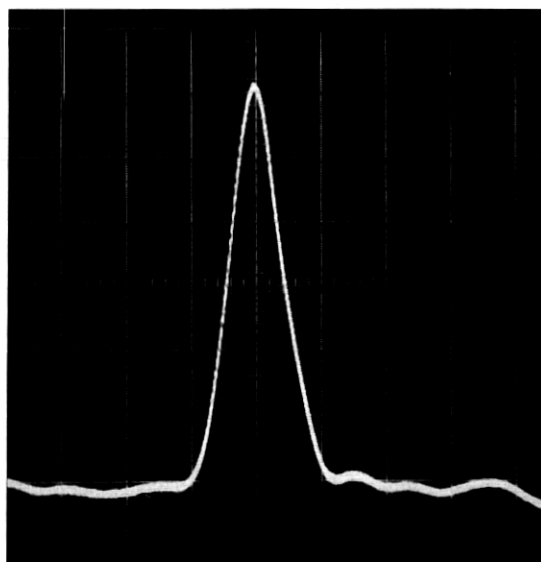

Fig. 25 — Pulse response of packaged diode at 50-volt back bias into 50-ohm load obtained from phase locked modes of He-Ne gas laser. Horizontal scale 0.5 nsec/cm, vertical scale 20 mvolt/cm.

Fig. 26 — Pulse response of Schottky barrier photodiode at 0-volt, 4-volt, 15-volt, and 50-volt back bias. Horizontal scale 1 nsec/cm, vertical scale 25 mvolt/cm.
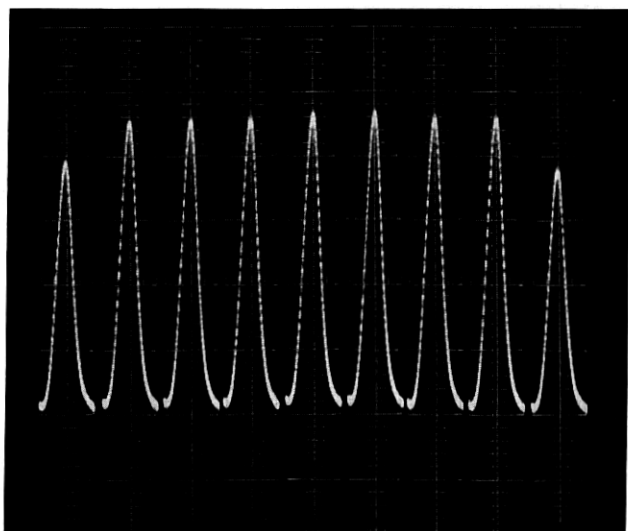

Fig. 27 — Pulse response for 9 points on the same photodiode obtained by linear scanning of a focused laser beam over diode area by 0.025-mm increments. Horizontal scale 2 nsec/cm, vertical scale 25 mvolt/cm.

Fig. 27 shows the pulse response of a Schottky barrier photodiode at various locations of the diode. A laser beam is focused on the front surface of the diode and is scanned across the diode. The pulse response is measured on an axis at discrete points which are spaced 1 mil apart. The peak variation is less than 3 percent over a total distance of 7 mils. The reduced pulse response in the vicinity of the boundaries is due to the fact that there is a small thickness change of the antireflection coating close to the boundary. This change of thickness is due to different sticking coefficients and different surface mobilities of the zinc sulfide on gold and on silicon during the evaporation process. One observes therefore a reduced amplitude response with no degradation of the pulse shape.

VIII. CONCLUSIONS

Schottky barrier photodiodes can be used for fast and efficient optical detectors. The high efficiency is obtained because radiation can be coupled through thin metal films with relatively low loss at optical frequencies. The small reflectance of the diode is achieved by proper choice of the matching layer. A diode with a fast response is obtained by designing junctions with a small RC product. The problem is similar to building high cutoff Schottky barriers for microwave and millimeter wave circuits. Additional limitations are due to transit time effects which are common to all solid-state radiation detectors based on carrier generation.

IX. ACKNOWLEDGMENTS

REFERENCES

1. Schottky, W., Semiconductor Theory of Blocking Layer and Point Contact Rectifier, Z. Physik, *113*, 1939, pp. 367–414.
2. Schottky, W. and Spenke, E., Zur quantitativen Durchführung der Raumladungs- und Randschichttheorie der Kristallgleichrichter, Wiss. Veröff. Siemens-Werken, *18*, 1939, pp. 225–291.
3. Kahng, D., Au-n-Type GaAs Schottky Barrier and Its Varactor Application, B.S.T.J., *43*, January, 1964, pp. 215–224.
4. Kahng, D. and D'Asaro, L. A., Gold-Epitaxial Silicon High-Frequency Diodes, B.S.T.J., *43*, January, 1964, pp. 225–232.

5. Irvin, J. C. and Young, D. T., Millimeter Frequency Conversion using Au-n-Type GaAs Schottky Barrier Epitaxial Diodes with a Novel Contacting Technique, Proc. IEEE, *53*, December, 1965, pp. 2130–2131.
6. Anderson, L. K., Photodiode Detection, Proc. Symp. Optical Masers, Microwave Research Institute Symposia Series, Polytechnic Institute of Brooklyn, *8*, April, 1963, pp. 549–566.
7. Lucovsky, G. and Emmons, R. B., High Frequency Photodiodes, Appl. Opt., *4*, June, 1965, pp. 697–702.
8. Riesz, R. P., High Speed Semiconductor Photodiodes, Rev. Sci. Instr., *33*, September, 1962, pp. 994–998.
9. Anderson, L. K., McMullin, P. G., D'Asaro, L. A., and Goetzberger, A., Microwave Photodiodes Exhibiting Microplasma-free Carrier Multiplication, Appl. Phys. Letters, *6*, February, 1965, pp. 62–64.
10. Melchior, H. and Lynch, W. T., Signal and Noise Response of High Speed Germanium Avalanche Photodiodes, IEEE Trans. Electron Devices, to be published.
11. Sharpless, W. M., Cartridge-Type Point-Contact Photodiode, Proc. IEEE, *52*, February, 1964, pp. 207–208.
12. Di Domenico, M., Sharpless, W. M.,and McNicol, J. J., High Speed Photodetection in Germanium and Silicon Cartridge-Type Point-Contact Photodiodes, Appl. Opt., *4*, June, 1965, pp. 677–682.
13. Schopper, H., *Landolt-Börnstein Zahlenwerte aus Physik, Chemie und Technik*, Springer-Verlag, Göttingen, *2*, Part 8, 1962, pp. 1–42.
14. Heavens, O. S., *Reports on Progress in Physics*, Institute of Physics and the Physical Society, London, *23*, 1960, pp. 1–65.
15. Mayer, H., *Physik Dünner Schichten*, Wissenschaftliche Verlagsgesellschaft, Stuttgart, Part 1, 1950, pp. 293–307.
16. Parker Givens, M., *Solid State Physics*, ed. by F. Seitz and D. Turnbull, Academic Press, Inc., New York, *6*, 1958, pp. 313–352.
17. Abelès, F., *Physics of Thin Films*, ed. by G. Hass and R. E. Thun, Academic Press, Inc., New York, *3*, 1965.
18. Bennett, J. M. and Ashley, E. J., Infrared Reflectance and Emittance of Silver and Gold Evaporated in Ultrahigh Vacuum, Appl. Opt. *4*, February, 1965, pp. 221–224.
19. Behrndt, K. H., *Deposition Processes for Thin Films, Techniques in Metals Research*, ed. by R. F. Bunshah, *1*, Interscience Publishers, New York, 1967.
20. Hall, A. C., Experimental Determination of the Optical Constants of Metals, J. Opt. Soc. Am., *55*, August, 1965, pp. 911–915.
21. Holland, L., *The Properties of Glass Surfaces*, John Wiley and Sons, Inc., New York, 1964, pp. 300–301.
22. Chopra, K. L., Influence of Electric Field on the Growth of Thin Metal Films, J. Appl. Phys., *37*, May, 1966, pp. 2249–2254.
23. Francombe, M. H. and Sato, H., *Single-Crystal Films*, The MacMillan Company, New York, 1964.
24. Wolter, H., *Optics of Thin Films, Encyclopedia of Physics*, *24*, Springer Verlag, Göttingen, 1956, pp. 461–473.
25. Fry, T. C., Plane Waves of Light, J. Opt. Soc. Am., *15*, September, 1927, pp. 137–161.
26. Fry, T. C., Plane Waves of Light, J. Opt. Soc. Am., *16*, January, 1928, pp. 1–25.
27. Perry, D. L., Low Loss Multilayer Dielectric Mirrors, Appl. Opt., *4*, August, 1965, pp. 987–995.
28. Kahng, D., Conduction Properties of the Au-n-Type-Si Schottky Barrier, Solid State Elec., *6*, May, 1963, pp. 281–295.
29. Cowley, A. M. and Sze, S. M., Surface States and Barrier Height of Metal-Semiconductor Systems, J. Appl. Phys., *36*, October, 1965, pp. 3212–3220.
30. Gärtner, W. W., Depletion Layer Photoeffects in Semiconductors, Phys. Rev., *116*, October 1, 1959, pp. 84–87.
31. DeLoach, B. C., personal communication.
32. Lucovsky, G. and Emmons, R. B., Lateral Effects in High-Speed Photodiodes, IEEE Trans. Electron Devices, *ED-12*, January, 1965, pp. 5–12.